# Ultra-cold atom quantum tunneling through single and double optical barriers

Roy Eid, Alfred Hammond, Lucas Lavoine, Thomas Bourdel

▶ **To cite this version:**

Roy Eid, Alfred Hammond, Lucas Lavoine, Thomas Bourdel. Ultra-cold atom quantum tunneling through single and double optical barriers. Physical Review A, 2024, 110, pp.043316. 10.1103/PhysRevA.110.043316 . hal-04584778v2

**HAL Id: hal-04584778**
**https://hal.science/hal-04584778v2**

Submitted on 12 Nov 2024

**HAL** is a multi-disciplinary open access archive for the deposit and dissemination of scientific research documents, whether they are published or not. The documents may come from teaching and research institutions in France or abroad, or from public or private research centers.

L'archive ouverte pluridisciplinaire **HAL**, est destinée au dépôt et à la diffusion de documents scientifiques de niveau recherche, publiés ou non, émanant des établissements d'enseignement et de recherche français ou étrangers, des laboratoires publics ou privés.

# Ultra-cold atom quantum tunneling through single and double optical barriers

R. Eid, A. Hammond, L. Lavoine, and T. Bourdel*
*Laboratoire Charles Fabry, CNRS, Institut d'Optique Graduate School, CNRS, Université Paris-Saclay, , 91127 Palaiseau, France*
(Dated: November 12, 2024)

We realize textbook experiments on Bose-Einstein condensate tunneling through thin repulsive potential barriers. In particular, we demonstrate atom tunneling though a single optical barrier in the quantum scattering regime where the de Broglie wavelength of the atoms is larger than the barrier width. Such a beam splitter can be used for atom interferometry and we study the case of two barriers creating an atomic Fabry-Pérot cavity. Technically, the velocity spread of the atoms is reduced due to the use of a $^{39}$K Bose-Einstein condensate with no interactions. The potential barriers are created optically and their width is tunable due to the use of a digital micro-mirror device. In addition, our scattering experiments enable *in situ* characterization of the optical aberrations of the barrier optical system.

Particle quantum tunneling is a phenomenon in which a particle passes through a potential energy barrier, which according to classical mechanics should not be passable due to insufficient energy. It is a direct consequence of the wave-nature of matter and is described by the Schrödinger equation [1]. Experimentally, it was first observed for electrons in semiconductors by L. Esaki [2], who then used this effect to build electronic diodes [3]. The scanning tunneling microscope is an important application based on quantum tunneling [4].

Equivalently, atoms can also exhibit quantum (wave) behavior, although they need to be cooled to ultralow temperatures. Ultracold atoms are indeed used both for precision measurements using matter-wave interferometers [5] or for the study of quantum many-body physics [6]. Tunneling of atoms between sites of an optical lattice [7] or of a double well-potential [8] is a commonly observed phenomenon. In a waveguide configuration in which the atoms move, beam splitting was realized through Bragg scattering [9], quantum reflection from the attractive potential close to a solid surface was observed [10, 11] and tunneling was studied in a transport experiment between two unbalanced fermionic reservoirs [12].

In the simple textbook experiment of an atom crossing a single potential barrier, the interesting regime of coherent splitting requires a barrier size $\sigma$ comparable to the atom de Broglie wavelength $\lambda_{\mathrm{dB}} = h/mv$, where $m$ is the atom mass, $v$ the atom velocity, and $h$ the Planck constant. Unless one uses an advanced technique to create sub-wavelength potential patterns [13], the minimum optical barrier size is limited by diffraction and it thus requires one to reduce and control $v$ to sub-millimeter per second velocities. As a consequence, there have been only a few experiments on quantum tunneling through optical barriers with a moving Bose-Einstein condensate (BEC) [14–18]. The low velocity thin barrier regime, characterized by $\lambda_{\mathrm{dB}} \gg \sigma$ and also called the quantum scattering regime, has never been directly observed. In contrast, numerous theoretical studies have explored atomic tunneling phenomena, considering various barrier shapes and incorporating interactions within BECs [19–21]. Matter-wave Fabry-Pérot interference using two consecutive barriers remains to be observed with potential applications for narrowing the atomic velocity distribution in precision measurements apparatus [22].

In the past ten years, digital micro-mirror devices (DMDs) have been shown to be a great tool to impose arbitrary potentials in ultracold-atom experiments [23–27]. For example, box traps permit one to study gases at a constant density [24, 27] and donut-shape traps are nice for the study of superfluid rotation [28]. Thanks to their versatility and the novel possibilities they offer, DMDs are increasingly used. The optical resolution of such setups is usually measured before their installation in the ultracold atom experiment and not characterized *in situ*.

In this paper we perform atom tunneling experiments through simple and double repulsive optical barriers. The barriers are generated through a DMD setup allowing the adjustment of the barrier width and position. The fine control of the atom velocity is achieved by using a $^{39}$K condensate that can be made non-interacting due to Feshbach tuning [29]. For single barriers, we are able to distinctly show the two different regimes of scattering. When $\lambda_{\mathrm{dB}} < \sigma$, the scattering is essentially classical. The transmission curve as a function of barrier height is close to a step function although rounded by quantum effects. When $\lambda_{\mathrm{dB}} > \sigma$, the transmission curve corresponds to the one expected for a $\delta$ potential. It is the quantum scattering regime. We then realize double barrier potentials. Interestingly, we observe oscillations of the transmission as a function of the distance between the two barriers. By comparison to numerical simulations, this behavior is interpreted as originating both from atomic Fabry-Pérot interference and from optical interference due to the oscillatory behavior of the point spread-function (PSF) of the optical

* Corresponding author: thomas.bourdel@institutoptique.fr

system. Interestingly, our results with various DMD patterns permit *in situ* characterization of the PSF.

The experiments start with the production of $^{39}K$ Bose-Einstein condensates in the $|F = 1, m_F = 1\rangle$ state by evaporation at 393 G, where the scattering length $a$ is $\sim$130 $a_0$ ( $a_0$ is the Bohr radius) in a crossed optical dipole trap [30]. The main horizontal optical trapping beam has a 40-$\mu$m waist, creating an atomic waveguide with cylindrical symmetry and the longitudinal confinement comes from a second optical beam with a 150-$\mu$m waist. The final preparation stage takes 100 ms in which the trap frequencies are modified from $(\omega_\perp, \omega_\parallel)/2\pi = (115, 47)$ Hz to $(\omega_\perp, \omega_\parallel)/2\pi = (120, 16)$ Hz, and the magnetic field is swept to 350 G in close proximity to the magnetic field where we observe collapse of the condensate due to the change of sign of the scattering length [31]. The gas is then almost non interacting [32]. When the second optical trap is switched off, we observe a very slow expansion of the condensate in the remaining optical waveguide, which corresponds to a mean energy of $h\times$8 Hz or equivalently to a velocity spread upon release $\Delta v_0 \sim 0.35$ mm/s [33]. This is only slightly higher than the kinetic energy $h\omega_\parallel/8\pi$ expected from a non-interacting condensate. There is also a residual $\sim$20% non condensed atomic fraction that expands much faster $\Delta v_{\rm thermal} \sim 2.6$ mm/s.

The optical barriers at 532 nm (Verdi V18, Coherent) are created with an optical setup using a digital micro-mirror devices (DLP-6500, Texas Instrument). The DMD is composed of a matrix of 1920x1080 small square mirrors of pitch size $p$ =7.56 $\mu$m. Each of them can take two different angles $\pm$12°. The DMD is illuminated by a large collimated beam at an angle of 24°. We then select only the most intense order of diffraction orthogonal to the DMD that corresponds to the specular reflection and image the DMD plane on the atoms through a custom-made objective. This objective is composed of three spherical lenses and has an overall focal length of 41.16 mm at 532 nm. The numerical aperture is 0.27. The distance from the DMD to the objective is 1.5 m such that the demagnification factor is 38.5 and the effective pixel size in the atomic plane is measured to be $p$=0.196 $\mu$m. The objective design takes into account the glass cell and theoretically gives perfect diffraction-limited performances and an Airy function as PSF. In the following, we use one-dimensional (1D) DMD patterns made of lines perpendicular to the propagation of the atoms. In that case, a more relevant quantity is the 1D amplitude PSF which is theoretically a sinc function. Given the numerical aperture, the first zero of the sinc function should theoretically correspond to $\sigma_{\rm th}$ =1.0 $\mu$m in the atomic plane (Fig. 1).

The experiment consists in releasing the Bose-Einstein condensate into the horizontal optical waveguide (by switching off the second optical trapping beam) and accelerating the atoms toward the optical barriers. The longitudinal acceleration is induced by a magnetic field gradient and is $g$ =0.40 m/s$^2$. The collision with

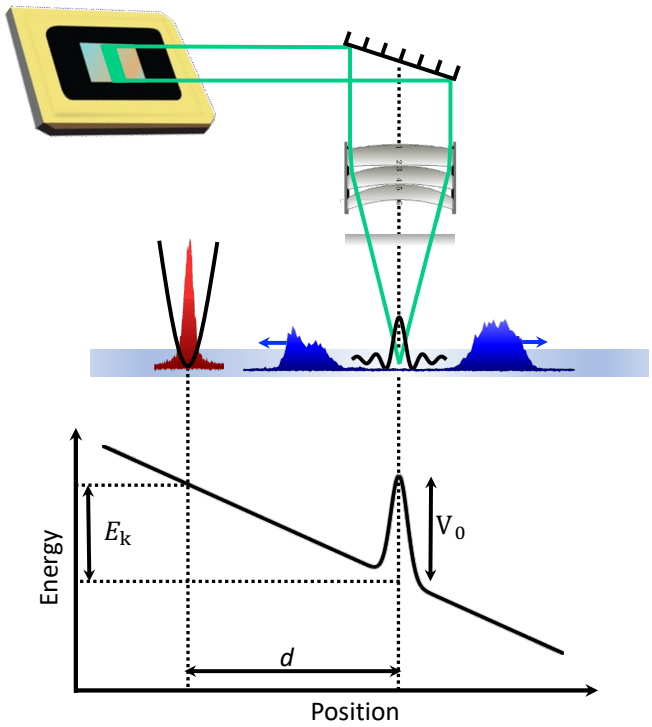


FIG. 1. Schematic of the experiment. A Bose-Einstein condensate is released and accelerated in an optical waveguide toward a potential barrier. This potential is made with a DMD optical setup at 532 nm. The measured quantities are the transmitted and reflected atom numbers after the collision when the two clouds are well separated. An example of a measured longitudinal density profile is shown.

a potential barrier results in partial reflection and transmission of the atomic cloud. The propagation time in the waveguide (between 15 and 30 ms) is chosen such that the atoms meet the barrier once and such that the reflected and transmitted atomic clouds are spatially full separated (Fig. 1). Finally, the main optical trap is switched off and the magnetic field is quickly brought to zero such that after a 1.3 ms time of flight the two transmitted and reflected atomic clouds are simultaneously imaged by fluorescence imaging. The transmission can thus be determined in a single realization of the experiment with no influence of the condensate atom number fluctuation. Choosing the distance $d$ from the initial trap to the barrier position (typ. between 15 and 100 $\mu$m), we control the speed of the atoms when they meet the barrier. We can also vary the barrier height through an acousto-optic modulator that modifies the 532 nm light power sent to the DMD. The barrier transmission can then be studied for different conditions. A key parameter is the ratio of the de Broglie wavelength of the atoms $\lambda_{\rm dB} = h/mv$ to the barrier width $\sigma$. Another important parameter is the atomic velocity spread $\Delta v$ when the atoms meet the barrier. Interestingly, since we keep the acceleration on for the whole sequence, $\Delta v$ is not directly given by $\Delta v_0$ [34]. The

kinetic energy of an atom with an initial velocity $v_0$ at a distance $d$ from the barrier is $E_k = \frac{1}{2}mv^2 = \frac{1}{2}mv_0^2 + mgd$. For our parameters, the second term dominates such that $v \approx \sqrt{2gd}$ and $\Delta v/v \approx \Delta x/2d \ll 1$ where $\Delta x \approx 3.5\,\mu$m is an estimated rms initial size of the cloud knowing the longitudinal trap frequency and the measured expansion energy.

We first focus on a case of high atom velocity 8.6 mm/s ($\lambda_{dB} = 1.2\,\mu$m) and a barrier made of ten pixels on the DMD, which corresponds to a size $\sigma_0 = 1.96\,\mu$m on the atoms. In that case, we expect diffraction and optical aberrations to only slightly enlarge the barrier width $\sigma \sim \sigma_0$. The transmission as a function of the barrier height is observed to be a step function although smoothed in the region of the transition (Fig. 2). Such a behavior is indeed expected in the classical regime, $\lambda_{dB} < \sigma$. The 50% transmission is then obtained when the barrier height $V_0$ corresponds to the kinetic energy of the atoms. The data can be directly compared to numerical simulations that consist in solving the 1D time-independent Schrödinger equation for an incoming plane wave. The ratio of the transmitted plane wave to the incoming plane wave amplitudes gives the transmission. The simulation globally matches the experimental data. The fact that the experimental transmission does not really span from 1 to 0 in our data is a consequence of thermal atoms whose behavior is not included in the simulation. For example, some thermal atoms due to their backward initial velocities have not encountered the barrier in the time of the experiment although they are counted as reflected.

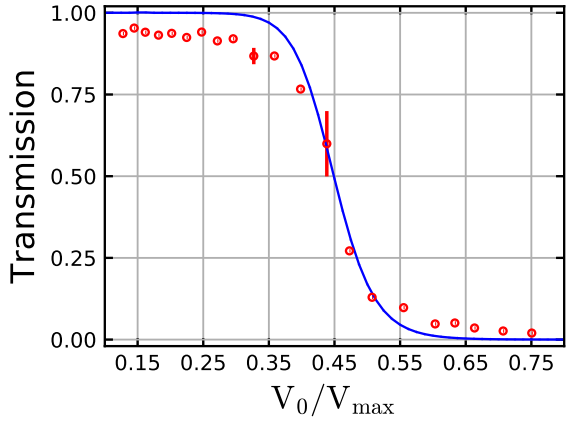


FIG. 2. Transmission in the classical regime $\sigma \sim 2\,\mu$m$> \lambda_{dB} = 1.2\,\mu$m. The transmission is plotted as a function of the barrier height $V_0$ that is normalized to its maximum value $V_{max}$ obtained at full laser power. The points are single shot experimental data. The solid line is the curve expected from simulations, with the theoretical sinc PSF and assuming no velocity spread of the atoms. The barrier height is the only fit parameter. Some typical statistical error bars are shown.

The previous results can be compared to the situation at low atom velocity 3.7 mm/s ($\lambda_{dB} = 3.0\,\mu$m) and a barrier made of three pixels on the DMD. The size of the potential barrier is then mostly given by the resolution of the imaging system. The transmission curve then qualitatively changes shape with a smooth decaying behavior. Such a behavior is expected in the quantum regime $\lambda_{dB} > \sigma$. In that case, the barrier width is not resolved by the atoms, the barrier can be theoretically replaced by a $\delta$ potential and the corresponding analytical transmission curve matches the experimental data. As previously, deviations from the theoretical transmission curve are probably coming from the thermal gas contribution (Fig. 3).

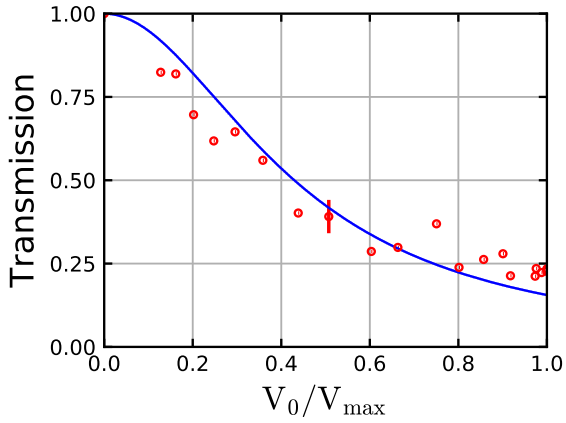


FIG. 3. Transmission in the quantum regime $\sigma \sim 1\,\mu$m$< \lambda_{dB} = 3.0\,\mu$m. The solid line corresponds to the expected transmission for a $\delta$ potential barrier $(1/(1+V_0^2/V_{ref}^2)$ and no velocity spread of the atoms. Here $V_{ref}$ is fitted to the data.

In both previous cases, the shape of the transmission curve is not very dependent on the actual PSF of the imaging system. Indeed, in the first case, the barrier width is dominated by the number of pixels creating the potential on the DMD, whereas in the quantum case, the width is not resolved by the atoms. In order to experimentally access the PSF and its width, we turn to a different experiment where we compare at a constant velocity (5 mm/s), the measured 532-nm power that is necessary to reflect 50% of the atoms for different barrier widths (Fig. 4). For our parameters (although we are not always strictly in the classical regime), the 50% transmission is numerically found to correspond to the situations where the barrier height equals the kinetic energy $V_0 = E_{kin}$. Such an experiment thus permits one to measure the relative barrier maxima for barriers made of different numbers of pixels $N_{pix}$ or equivalently of different width $\sigma_0$. The exact barrier shape is the absolute value square of the convolution of the amplitude PSF with door functions of variable width $\sigma_0 = N_{pix}p$. In the limit of small $\sigma_0$, the barrier maximum is proportional to $\sigma_0^2$ as the field interferes constructively. In this case, the 50% transmission power scales as $1/\sigma_0^2$. On the contrary, for large barrier size, we expect the barrier maximum height and thus also the

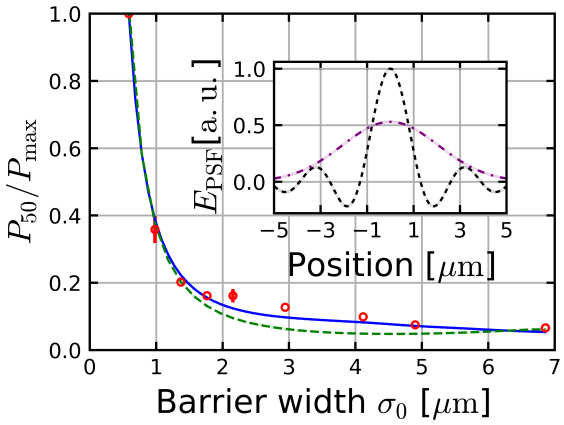


FIG. 4. Optical power $P_{50}$ needed to reflect 50% of the atoms as a function of the barrier width $\sigma_0$. The optical power is normalized to its maximum value $P_{\max}$. The mean atomic velocity is 5 mm/s, corresponding to a $\lambda_{\mathrm{dB}} = 2.0\,\mu$m. The dashed (solid) line corresponds to the numerical result with a sinc PSF with $\sigma_{\mathrm{res}} = 2.0\,\mu$m (the ansatz PSF). The real (dash-dotted line) and imaginary (dotted line) parts of the ansatz PSF are plotted in the inset (see the textfor details).

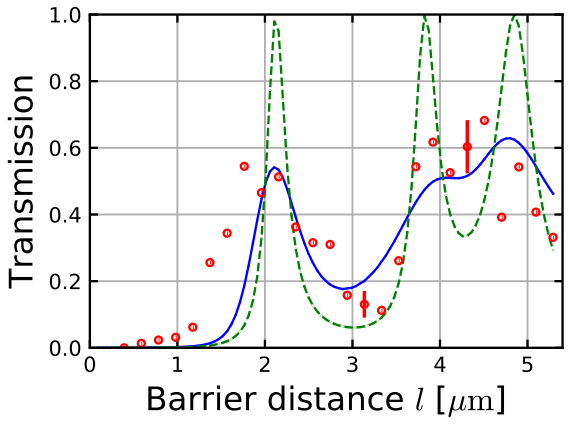


FIG. 5. Transmission through two barriers as a function of the distance between them. The mean atomic velocity is $\sim$ 3.3 mm/s ($\lambda_{\mathrm{dB}} = 3.1\,\mu$m). The solid line is the numerical solutions with the ansatz PSF (see the text for details) and a velocity spread $\Delta v = 0.25$ mm/s. The dashed line is the numerical solution for monokinetic atoms. In this last case, the Fabry-Pérot resonance peaks are resolved.

50% transmission power to be independent of $\sigma_0$. These two limiting behaviors are experimentally observed (Fig. 4). The change of behavior occurs when the resolution of the imaging system is of the order of $\sigma_0$. Assuming a sinc PSF with a resolution $\sigma_{\mathrm{res}}$, we can calculate the barrier maximum for each barrier width $\sigma_0$. We find that in order to reproduce the observed power ratio between the two limiting regimes, we need $\sigma_{\mathrm{res}} \approx 2\sigma_{\mathrm{th}} = 2.0\,\mu$m (dashed curve in Fig. 4). However, the whole curve is not well fitted, in particular for barrier widths between 2 and 5 $\mu$m. Our results thus point toward a PSF modified by optical aberrations, i.e. not a sinc function. The consideration of a more complex PSF as presented below permits us to better match the observation (solid curve in Fig. 4).

We now turn to transmission experiments through double barriers. In this series of experiments, we use a velocity of 3.3 mm/s, barrier widths of two pixels and 75% of the maximum power available. For such parameters, the transmission through a single barrier is $\sim$70%. We then vary the distance $l$ between the two barriers and, as previously, study the transmission (Fig. 5). Interestingly, the transmission shows oscillations as a function of the barrier distance. However, one should be careful in directly interpreting them as Fabry-Pérot peaks. First, in contradiction to the expectation, they do not reach 100% transmission. Second, the peaks are not precisely positioned at multiples of $\lambda_{\mathrm{dB}}/2$. Note that for larger barrier distances, the transmission is essentially constant to $\sim$ 50% [35].

In order to interpret our data, two important ingredients have to be taken into account. First, the atoms have a velocity spread that can eliminate interference effects. It can be estimated to $\Delta v = 0.25$ mm/s from the experimental parameters and can be considered in simulations by averaging the transmission over the velocity distribution. Second the studied barrier distances are not much larger than the resolution of the optical system. We should thus take into account that the barriers have some width and moreover that the optical fields originating from the two DMD regions may interfere as we use coherent light. In principle, the exact calculation of the optical profile requires the knowledge of the amplitude PSF of the optical objective (with its real and imaginary parts), which differs from the theoretical one. In preliminary measurements, prior to the installation on the atoms, the image of a point source (corresponding to the intensity PSF) appeared to be diffraction limited up to a numerical aperture of $\sim 0.15$. The outer part of the objective only marginally contributed to the reduction of the size of the central image spot and was rather observed to add a broad background. We attribute this effect to imperfectly manufactured (non-spherical) lenses. A reasonable ansatz ampltitude PSF is thus a sinc function originating from the central part of the objective in addition to a Gaussian broader background originating from the outer part of the objective. For simplicity and because there is no reason to assume a given phase relation between the two components, we chose the Gaussian component to be imaginary such that there is no interference with the real sinc function.

With such an ansatz, we can calculate the optical potential and simulate the experimental transmission. We then adjust the PSF parameters to reproduce the experimental findings of both Fig. 4 and 5. We find that the amplitude PSF $\mathrm{E_{PSF}} \propto \mathrm{sinc}(\pi x/\sigma_{\mathrm{sinc}}) +$

$iA_{\rm G}\exp(-x^2/2\sigma_{\rm G}^2)$ with $\sigma_{\rm res} = 1.30\,\mu$m, $\sigma_{\rm G} = 2.07\,\mu$m, and $A_{\rm G} = 0.53$ (see the inset in Fig. 4) permits us to reasonably match the data (Fig. 4 and 5). Although, the actual PSF certainly differ from our ansatz, we expect the latter to capture its main features such as its size and its negative real part. Using the previous ansatz PSF, we also plot in Fig. 5, the expected transmission for monokinetic atoms. In that case, the transmission does reach 100% for specific barrier distance corresponding to Fabry-Pérot resonances. The precise resonance positions depend on the atom velocity, leading to a broadening of the transmission peaks after velocity averaging. This sensitivity to the velocity increases as a higher-order Fabry-Pérot resonance (at larger barrier distance) is considered. We thus find that the first Fabry-Pérot resonance peak is resolved but not the second and third ones which merge into a single broad peak. Note also that the monokinetic resonance peaks are not equally spaced. This is due to optical interference between the optical fields originating from the different areas on the DMD. The precise potential barrier heights and positions are slightly affected by the positive to negative oscillations of the amplitude PSF. In particular, for a barrier distance of $\sim 1.9\,\mu$m ($\sim 3.2\,\mu$m), the barrier heights are minimum (maximum), because the sinc function is maximally negative (positive) at those distances. Overall, we thus attribute the observed oscillations in the transmission to a combination of Fabry-Pérot interference and optical interference due to an oscillatory PSF.

In conclusion, we have realized several textbook experiments on atomic transmission through optical barriers. Key advantages of our experiments are the use of non interacting Bose-Einstein condensates and a digital micro-mirror device for the tuning of the barrier characteristics. We clearly demonstrated both the classical and quantum regimes of atomic scattering on a single optical barrier by adjusting both the barrier width and the de Broglie wavelength, or equivalently, the speed of the atoms. We then realized an atomic Fabry-Pérot interferometer based on two potential barriers and were able to resolve the first Fabry-Pérot resonance peak. Interestingly, our setup using a DMD to produce the optical barriers allows for experiments with varying barrier widths and distances permitting an *in situ* estimation of the PSF of the optical system. Technical improvements, such as further reduction of the atom velocity spread using delta-kick cooling technique [36] and/or the engineering of moving barriers using the high switching rate capabilities of DMDs [37, 38] could lead to the observation of a complete atom Fabry-Pérot resonator spectrum.

In the future, the capacity to realize coherent beam splitters from single barriers could be important in the context of atom interferometry. A matter-wave Fabry-Pérot interferometer acting as a gravimeter has been proposed [39]. In addition, our results open prospects for the study of the influence of interactions on collisions with potential barriers [19–21]. Scattering of a bright soliton on a barrier has been predicted to lead to non-classical NOON states [40–43]. In the case of a Fabry-Pérot interferometer, interactions are expected to lead to quantum effects such as squeezing of the outgoing atomic cloud or atomic blockade [44].

This research was supported by CNRS, Ministère de l'Enseignement Supérieur et de la Recherche, Labex PALM, Quantum Paris-Saclay, Région Ile-de-France in the framework of Domaine d'Intérêt Majeur Quantip, Paris-Saclay in the framework of IQUPS, ANR Droplets (Grant No. 19-CE30-0003), and the Simons Foundation (Award No. 563916, localization of waves).

[1] D.J. Griffiths, *Introduction to Quantum Mechanics* (Pearson Prentice Hall, 1995).
[2] L. Esaki, Long journey into tunneling, Nobel Lecture, available at https://www.nobelprize.org/-prizes/physics/1973/esaki/lecture/ (1973).
[3] L. Esaki, New phenomenon in narrow germanium *p-n* junctions, Physical Review A **109**, 603 (1958).
[4] G. Binnig, H. Rohrer, C. Gerber, and E. Weibel, Tunneling through a controllable vacuum gap, Applied Physics Letters **40**, 178 (1982).
[5] A.D. Cronin, J. Schmiedmayer, and D.E. Pritchard, Optics and interferometry with atoms and molecules, Rev. Mod. Phys. **81**, 1051 (2009).
[6] I. Bloch, J. Dalibard, and W. Zwerger, Many-body physics with ultracold gases, Rev. Mod. Phys. **80**, 885 (2008).
[7] M. Greiner, O. Mandel, T. Esslinger, T. Hänsch, and I. Bloch, Quantum phase transition from a superfluid to a Mott insulator in a gas of ultracold atoms, Nature **415**, 39 (2002).
[8] M. Albiez, R. Gati, J. Fölling, S. Hunsmann, M. Cristiani, and M. K. Oberthaler, Direct observation of tunneling and nonlinear self-trapping in a single bosonic josephson junction, Phys. Rev. Lett. **95**, 010402 (2005).
[9] C. M. Fabre, P. Cheiney, G. L. Gattobigio, F. Vermersch, S. Faure, R. Mathevet, T. Lahaye, and D. Guéry-Odelin, Realization of a distributed bragg reflector for propagating guided matter waves, Phys. Rev. Lett. **107**, 230401 (2011).
[10] T. A. Pasquini, Y. Shin, C. Sanner, M. Saba, A. Schirotzek, D. E. Pritchard, and W. Ketterle, Quantum reflection from a solid surface at normal incidence, Phys. Rev. Lett. **93**, 223201 (2004).
[11] F. Shimizu, Specular reflection of very slow metastable neon atoms from a solid surface, Phys. Rev. Lett. **86**, 987 (2001).
[12] S. Häusler, S. Nakajima, M. Lebrat, D. Husmann, S. Krinner, T. Esslinger, and J.-P. Brantut, Scanning gate microscope for cold atomic gases, Phys. Rev. Lett. **119**, 030403 (2017).
[13] Y. Wang, S. Subhankar, P. Bienias, M. Lacki, T.-C. Tsui, M. A. Baranov, A. V. Gorshkov, P. Zoller, J. V.

Porto, and S. L. Rolston, Dark state optical lattice with a subwavelength spatial structure, Phys. Rev. Lett. **120**, 083601 (2018).
[14] T.A. Pasquini, M. Saba, G.B. Jo, Y. Shin, W. Ketterle, D.E. Pritchard, T.A. Savas, and N. Mulders, Low velocity quantum reflection of Bose-Einstein condensates, Physical Review Letters **97**, 093201 (2006).
[15] A.L. Marchant, T.P. Billam, M.M.H. Yu, A. Rakonjac, J.L. Helm, J. Polo, C. Weiss, S.A. Gardiner, and S.L. Cornish, Quantum reflection of bright solitary matter waves from a narrow attractive potential, Phys. Rev. A **93**, 021604(R) (2016).
[16] J. Billy, V. Josse, Z. Zuo, W. Guerin, A. Aspect, and P. Bouyer, Guided atom laser: a new tool for guided atom optics, Ann. de Phys. (France) **32**, 17 (2007).
[17] R. Ramos, D. Spierings, S. Potnis, and A.M. Steinberg, Atom-optics knife edge: Measuring narrow momentum distributions, Phys. Rev. A **98**, 023611 (2018).
[18] R. Ramos, D. Spierings, I. Racicot, and A.M. Steinberg, Measuring the time a tunnelling atom spends in the barrier (2019).
[19] A.M. Martin, R.G. Scott, and T.M. Fromhold, Transmission and reflection of Bose-Einstein condensates incident on a Gaussian tunnel barrier, Physical Review A **75**, 065602 (2007).
[20] P. Manju, K.S. Hardman, M.A. Sooriyabandara, P.B. Wigley, J.D. Close, N.P. Robins, M.R. Hush, and S.S. Szigeti, Quantum tunneling dynamics of an interacting Bose-Einstein condensate through a Gaussian barrier, Physical Review A **98**, 053629 (2018).
[21] D.R. Lindberg, N. Gaaloul, L. Kaplan, J.R. Williams, D. Schlippert, P. Boegel, E.-M. Rasel, and D.I. Bondar, Asymmetric tunneling of Bose–Einstein condensates, J. Phys. B **56**, 025302 (2023).
[22] P. Manju, K.S. Hardman, P.B. Wigley, J.D. Close, N.P. Robins, and S.S. Szigeti, An atomic Fabry–Perot interferometer using a pulsed interacting Bose-Einstein condensate, Scientific Reports **10**, 15052 (2020).
[23] J. Liang, R. Kohn, Jr., M. Becker, and D. Heinzen, 1.5% root-mean-square flat-intensity laser beam formed using a binary-amplitude spatial light modulator, Appl. Opt. **48**, 1955 (2009).
[24] A.L. Gaunt, T.F. Schmidutz, I. Gotlibovych, R.P. Smith, and Z. Hadzibabic, Bose-Einstein condensation of atoms in a uniform potential, Phys. Rev. Lett. **110**, 200406 (2013).
[25] G. Gauthier, I. Lenton, N. Parry, M. Baker, M.J. Davis, H. Rubinsztein-Dunlop, and T.W. Neely., Direct imaging of a digital-micromirror device for configurable microscopic optical potentials, Optica **3**, 1136 (2016).
[26] M. Tajik, B. Rauer, T. Schweigler, F. Cataldini, J. Sabino, F.S. Møller, S.-C. Ji, I.E. Mazets, and J. Schmiedmayer, Designing arbitrary one-dimensional potentials on an atom chip, Opt. Express **27**, 33474 (2019).
[27] N. Navon, R.P. Smith, and Z. Hadzibabic, Quantum gases in optical boxes, Nature Physics **17**, 1334 (2021).
[28] Y.-Q. Zou, É.L. Cerf, B. Bakkali-Hassani, C. Maury, G. Chauveau, P.C.M. Castilho, R. Saint-Jalm, S. Nascimbene, J. Dalibard, and J. Beugnon, Optical control of the density and spin spatial profiles of a planar Bose gas, Journal of Physics B **54**, 08LT01 (2021).
[29] C. D'Errico, M. Zaccanti, M. Fattori, G. Roati, M. Inguscio, G. Modugno, and A. Simoni, Feshbach resonances in ultracold 39K, New Journal of Physics **9**, 223 (2007).
[30] G. Berthet, L. Lavoine, M.K. Parit, A. Brolis, A. Boissé, and T. Bourdel, Observation of the algebraic localization-delocalization transition in a one-dimensional disordered potential with a bias force, Phys. Rev. Res. **2**, 013386 (2020).
[31] E. Donley, N. Claussen, S. Cornish, J. Roberts, E. Cornell, and C. Wieman, Dynamics of collapsing and exploding Bose-Einstein condensates, Nature **402**, 295 (2001).
[32] In this regime of very low scattering length $a < 0.3\,a_0$, the magnetic dipole interaction plays a role comparable to the contact interaction.
[33] We also observe uncontrolled shot-to-shot fluctuations of the mean velocity with a standard deviation of 0.23 mm/s, that we attribute to residual longitudinal dipole oscillations of the cloud prior to release. These are probably the main source of shot-to-shot fluctuation in our transmission data.
[34] F. Damon, F. Vermersch, J. G. Muga, and D. Guéry-Odelin, Reduction of local velocity spreads by linear potentials, Phys. Rev. A **89**, 053626 (2014).
[35] The potential gradient is kept on during the whole sequence. The influence of such a gradient has been studied theoretically [39]. It is expected to play little role in the presented data at small barrier distances and it is not taken into account in our simulations.
[36] H. Ammann and N. Christensen, Delta kick cooling: A new method for cooling atoms, Phys. Rev. Lett. **78**, 2088 (1997).
[37] L.-C. Ha, L.W. Clark, C.V. Parker, B.M. Anderson, and C. Chin, Roton-maxon excitation spectrum of Bose condensates in a shaken optical lattice, Phys. Rev. Lett. **114**, 055301 (2015).
[38] G. Gauthier, T. Bell, A. Stilgoe, M. Baker, H. Rubinsztein-Dunlop, and T. Neely, Dynamic High-Resolution Optical Trapping of Ultracold Atoms (Advances In Atomic, Molecular, and Optical Physics, Academic Press, Vol. 70, 2021) pp. 1–101.
[39] P. Schach, A. Friedrich, J. Williams, W. Schleich, and E. Giese, Tunneling gravimetry, EPJ Quant. Tech. **9**, 20 (2022).
[40] C. Weiss and Y. Castin, Creation and detection of a mesoscopic gas in a nonlocal quantum superposition, Phys. Rev. Lett. **102**, 010403 (2009).
[41] S.L. Cornish, N.G. Parker, A.M. Martin, T.E. Judd, R.G. Scott, T.M. Fromhold, and C.S. Adams, Quantum reflection of bright matter-wave solitons, Physica D: Nonlinear Phenomena **238**, 1299 (2009).
[42] A. Boissé, G. Berthet, L. Fouché, G. Salomon, A. Aspect, S. Lepoutre, and T. Bourdel, Nonlinear scattering of atomic bright solitons in disorder, EPL **117**, 10007 (2017).
[43] P. Naldesi, J. Polo, P.D. Drummond, V. Dunjko, L. Amico, A. Minguzzi, and M. Olshanii, Massive particle interferometry with lattice solitons, SciPost Phys. **15**, 187 (2023).
[44] I. Carusotto, Nonlinear atomic Fabry-Perot interferometer: From the mean-field theory to the atom blockade effect, Phys. Rev. A **63**, 023610 (2001).